Supplementary Information (SI)

Temperature-Driven Journey of Dark Excitons to Efficient Photocatalytic Water Splitting in β-AsP

Harshita Seksaria, Amal Kishore, Abir De Sarkar*

Institute of Nano Science and Technology, Knowledge City, Sector 81, Manauli, Mohali, Punjab 140306, India

Email: abir@inst.ac.in, abirdesarkar@gmail.com

Contents

Dynamical, mechanical and thermodynamical stability

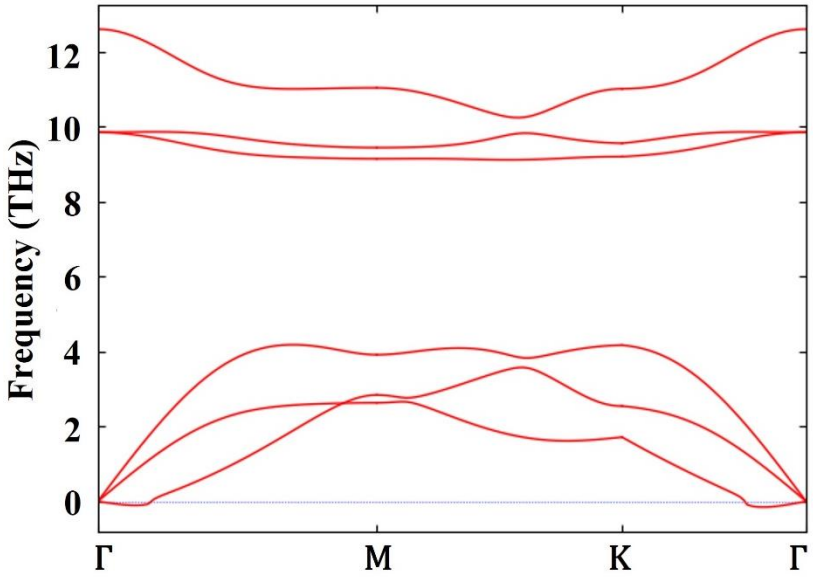

Figure S1. The phonon dispersion of blue-AsP with a supercell of 6x6x1

A small pocket of imaginary frequency ($\sim -0.18\ THz$) is observed around the Γ point in the acoustic flexural (ZA) mode, which is a mere artifact commonly observed in 2D materials and is extremely sensitive to the details of the calculations and in some cases, it goes off altogether with a bigger supercell and/or a denser k-mesh. It simply shows the difficulty in reaching numerical convergence for the acoustic flexural phonon mode, which happens to be a common issue in ab initio calculations on 2D materials. The small pockets of negative frequency (<0.3 THz or 10 cm^{-1}) around the Γ point arising from the flexural acoustic (ZA) modes have also been observed in graphene, silicone, molybdenum disulfide, indium and gallium chalcogenides[1,2]. This region of instability is particularly dependent on simulation parameters, such as supercell size and k-point sampling, and can be reduced by using a bigger supercell, denser k-mesh or including non-analytical correction (NAC) term.

Further, the Born-Huang stability criteria, which state that $C_{11}C_{22} - C_{12}^2 > 0$ and $C_{66} > 0$, are satisfied by the elastic constants of blue-AsP monolayer (C_{11}=C_{22}=67.74 N/m, C_{12}= C_{21}=11.39 N/m, C_{66}=28.18 N/m) affirming the mechanical stability of these materials.

The cohesive energies have been calculated using the following formula/equation:

$$E_{coh} = \frac{n_{As}E_{As} + n_P E_P - E_{AsP}}{n_{As} + n_P} \quad (1)$$

The thermodynamical stability of blue-AsP is justified by its positive cohesive energy, 4.87 eV, which is in agreement with the previously reported values[1].

The mechanical properties were explored to determine the angle-dependent Young's modulus and Poisson Ratio utilizing the following relations:

$$Y(\theta) = \frac{C_{11}C_{22} - C_{12}^2}{C_{11}sin^4\theta + C_{22}cos^4\theta + \left(\frac{C_{11}C_{22} - C_{12}^2}{C_{66}} - 2C_{12}\right)cos^2\theta sin^2\theta} \quad (2)$$

$$\nu(\theta) = \frac{C_{12}(cos^4\theta + sin^4\theta) - \left(C_{11}+C_{22} - \frac{C_{11}C_{22} - C_{12}^2}{C_{66}}\right)cos^2\theta sin^2\theta}{C_{11}sin^4\theta + C_{22}cos^4\theta + \left(\frac{C_{11}C_{22} - C_{12}^2}{C_{66}} - 2C_{12}\right)cos^2\theta sin^2\theta} \quad (3)$$

Here, C_{11}, C_{12}, C_{22}, and C_{66} are the elements of the elastic moduli matrix, and θ is the angle. Figure 3 visually exhibits traces of minute mechanical anisotropy, that may result in potential variations in material properties along different directions.

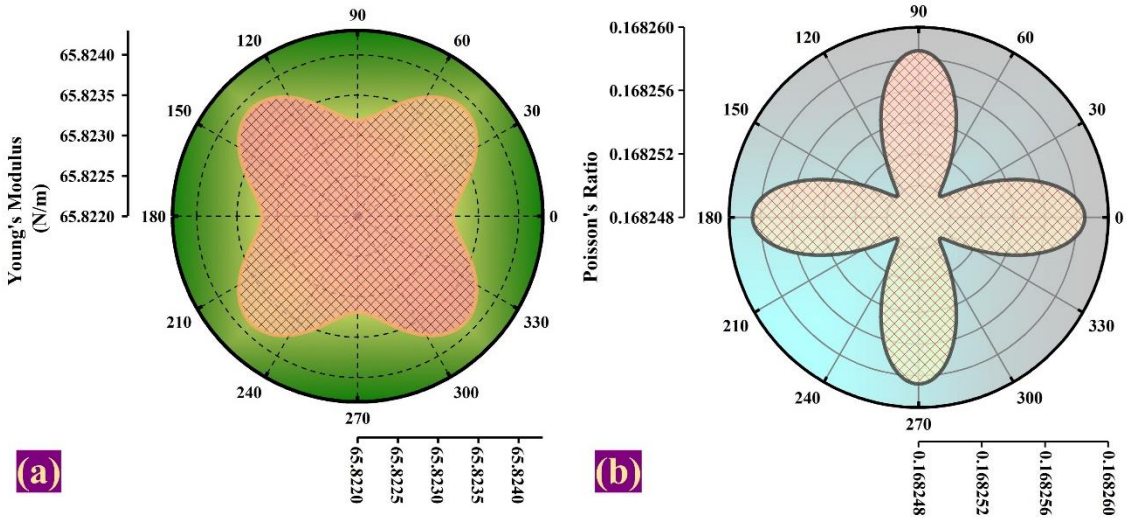

Figure S2. Minute mechanical anisotropy in blue AsP given by (a) Young's Modulus (b) Poisson's ratio

Thermal Stability at different temperatures

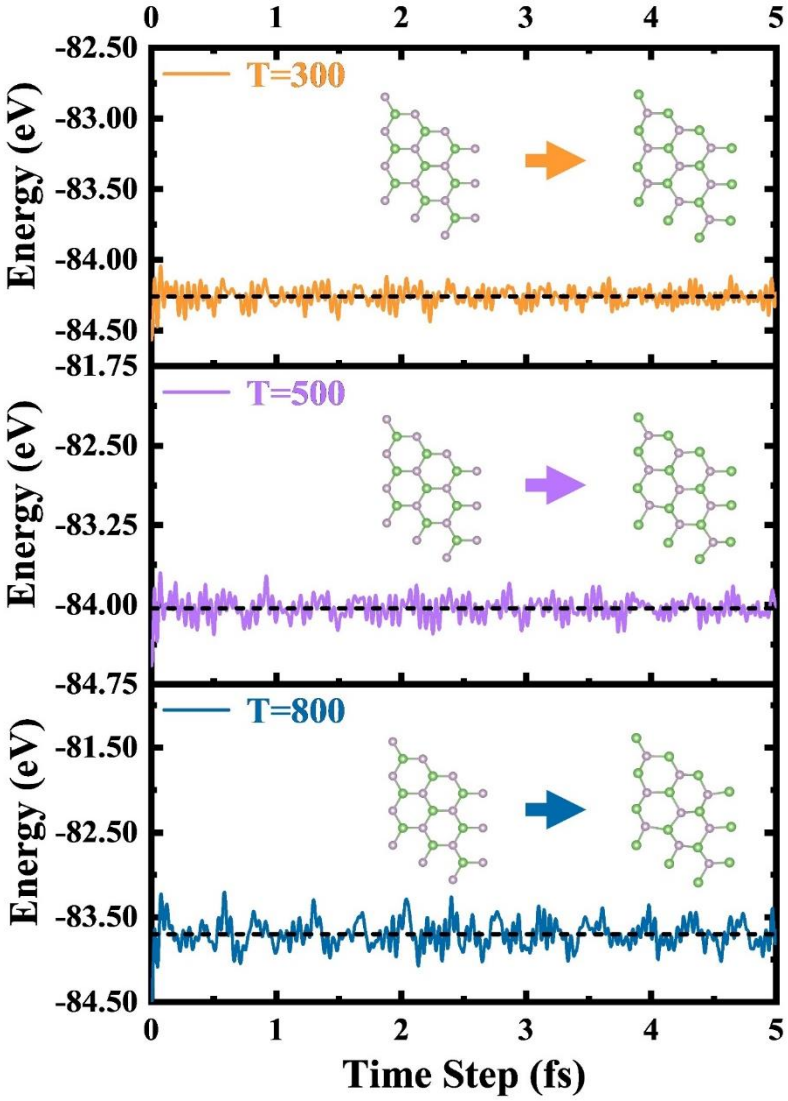

Figure S3. Ab initio molecular dynamics (AIMD) simulation at T=300 K, 500 K and 800 K for the time step of 5 ps for β −AsP. The before simulation and after simulation snapshots of the system has been shown.

Details of exciton lifetime calculations

Bethe Salpeter approach with Fermi's golden rule

Fermi's golden rule, based on first-order perturbation theory, describes the transition rate in a quantum system as a function of the transition matrix element and the density of states, which is given as follows:

$$\gamma_i^f = \frac{2\pi}{\hbar}|\langle i|H'|f\rangle|^2\delta\left(E_f - E_i - \hbar\omega\right) \quad (4)$$

This transition is driven by a perturbation

$$H' = -\frac{e}{mc}\mathbf{A}\cdot\mathbf{p}\ ;\ \mathbf{A} = \mathbf{A}_0\hat{\mathbf{e}}(\exp\left[i(\mathbf{k}\cdot\mathbf{r}-\omega t)\right] + \exp\left[-i(\mathbf{k}\cdot\mathbf{r}-\omega t)\right]) \quad (5)$$

where **p** is momentum and **A** the vector potential in second quantized form, $|i\rangle$ represents the initial state, and $|f\rangle$ represents the final state. Fermi's golden rule is also known as the decay probability, which is related to the inverse of the lifetime.

The transition rate γ_i^f is therefore proportional to the dipole matrix element:

$$\gamma_i^f = \frac{2\pi}{\hbar}\frac{e^2}{m^2c^2}A_0^2\sum\left|\langle v\mathbf{k}\left|e^{(i\mathbf{k}\cdot\mathbf{r})}\hat{\mathbf{e}}\cdot\mathbf{p}\right|c\mathbf{k}\rangle\right|^2\delta\left(E_f - E_i - \hbar\omega\right) \quad (6)$$

$$\gamma_i^f \propto \sum_{\mathbf{k}} |\langle v\mathbf{k}|\hat{\mathbf{e}}\cdot\mathbf{r}|c\mathbf{k}\rangle|^2 \propto p_s^2 \quad (7)$$

Bethe Salpeter equation gives the oscillator strength (μ_s) directly related to dipole matrix element p_s^2 as:

$$p_s^2 = \frac{m^2E_s(0)^2\mu_s^2}{\hbar^2} \quad (8)$$

where m is the effective mass and $E_s(0)$ is the excitation energy at zero momentum.

Effective exciton lifetime

The recombination rate of electron-hole pair at zero momentum, $\gamma_s(0)$ and therefore, the exciton lifetime (τ) at temperature T can be obtained by using the following relations[2]:

$$\gamma_s(0) = \frac{e^2p_s^2}{\varepsilon_0m^2cAE_s(0)} \quad (9)$$

$$\tau = \{\gamma_s(0)\}^{-1}\frac{3}{4}\left(\frac{2M_sc^2k_BT}{E_s(0)^2}\right) \quad (10)$$

where ε_0 is the absolute permittivity of free space, e is the charge of an electron, *A* is the area of the unit cell and M_s is the total effective mass.

Strain engineering of photogenerated charge carrier potential

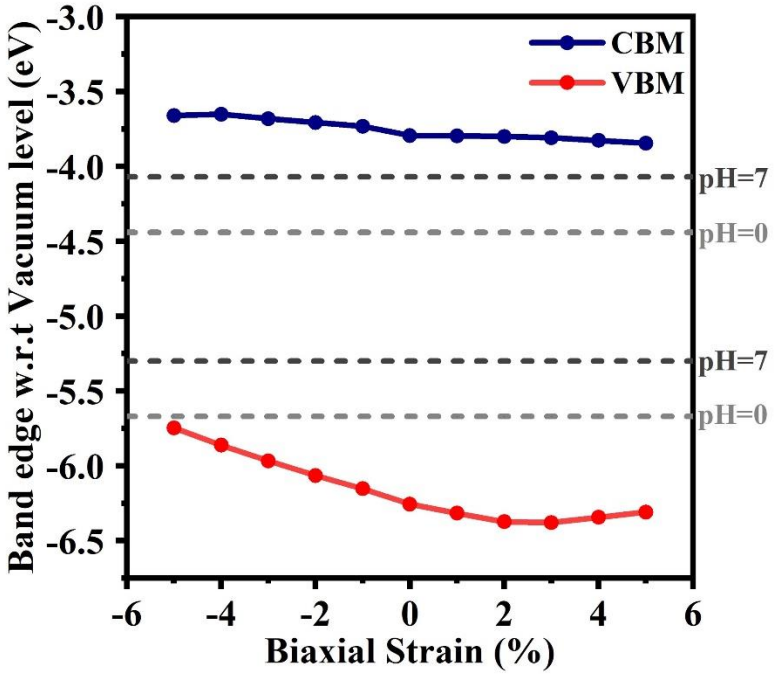

Figure S4. Band edges of blue-AsP varying with strain in absolute vacuum scale

Details of Gibbs free energy calculations

The primary determinant for a reaction to be thermodynamically favorable is a negative Gibbs free energy. The Gibbs free energy for each step in the two half-reactions (OER and HER) is determined using the following equation:

$$\Delta G = \Delta E + \Delta ZPE - T\Delta S + \Delta G_U + \Delta G_{pH} \quad (11)$$

where ΔE and ΔZPE represent the adsorption and the zero-point energy for each step. $T\Delta S$ denotes the entropy contribution at room temperature, i.e., $T = 298K$, and $\Delta G_U = -eU$ with e =elementary positive charge and U representing the potential bias which is taken as the sum of PCC potential and the external biasing potential. The determination of zero-point energy and the correction for entropy in energy relies on the utilization of vibrational frequencies, as outlined below:

$$ZPE = \frac{1}{2}\sum h\nu_i \quad (12)$$

$$TS_\nu = k_B T\left[\sum_K ln\left(\frac{1}{1-e^{-h\nu/k_BT}}\right) + \sum_K \frac{h\nu}{k_BT}\left(\frac{1}{e^{-h\nu/k_BT}-1}\right) + 1\right] \quad (13)$$

Furthermore, ΔG_{pH} accounts for the influence of pH on the energy of a step and is calculated as $\Delta G_{pH} = -k_B T ln10 \times pH$ when a non-zero pH is present. [3,4] The overall water redox reaction [$2H_2O \rightarrow O_2 + 4H^+$] in absence of any catalyst has a Gibbs free energy of 4.92 eV, indicating its highly endothermic nature and unfavourable conditions. However, by utilizing a catalyst, this reaction can be broken down into four individual elementary steps. In an ideal scenario with an ideal catalyst, each step would possess a Gibbs free energy of $(4.92/4) = 1.23\ eV$, requiring an external potential of 1.23 V. In practice, when a catalyst is present, certain reaction steps might demand a higher potential than the ideal per step reaction potential of 1.23 V. As a result, the Gibbs free energy per step becomes uneven. The deviation of the Gibbs free energy per step from the ideal step, or the minimum potential necessary in excess of the ideal potential per reaction step where all steps are thermodynamically favorable, is referred to as the theoretical overpotential for the oxygen evolution reaction (OER). This overpotential can be calculated using the following equation:

$$\boldsymbol{\eta_{OER} = \frac{[max(\Delta G_1, \Delta G_2, \Delta G_3, \Delta G_4) - 1.23eV]}{e}} \qquad (14)$$

where $\boldsymbol{\Delta G_1 = G_{OH},\ \Delta G_2 = G_O - G_{OH},\ \Delta G_3 = G_{OOH} - G_O, and\ \Delta G_4 = 4.92 - G_{OOH}}$ are the Gibbs potentials for the four steps of the OER process (Table S1) followed as:

$$\boldsymbol{R1:\ H_2O + * \rightarrow OH^* + e^- + H^+}$$

$$\boldsymbol{R2:\ OH^* \rightarrow O^* + e^- + H^+}$$

$$\boldsymbol{R3:\ H_2O + O^* \rightarrow HOO^* + e^- + H^+}$$

$$\boldsymbol{R4:\ HOO^* \rightarrow * + O_2 + e^- + H^+}$$

By introducing this overpotential as an external bias to the system, all the reaction steps will undergo thermodynamically favourable changes, leading to a downhill progression.

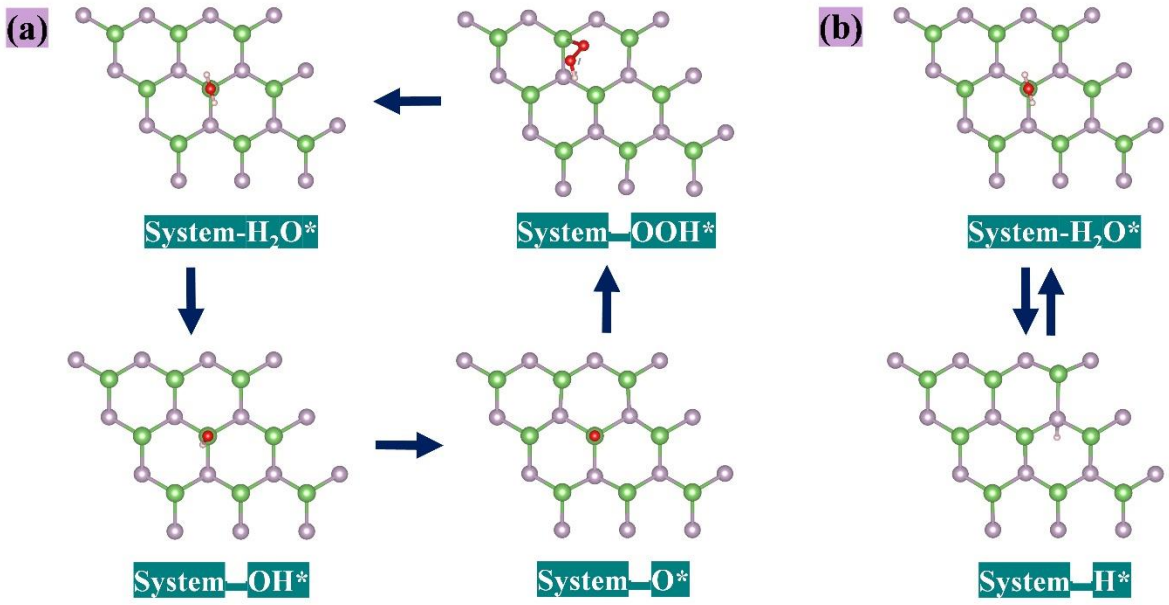

Figure S5. Reaction intermediates of blue-AsP during (a) OER and (b) HER. No significant geometrical changes are observed in the system.

Table S1. The Gibbs free energy ΔG_i for reaction steps and the overpotential η(V). The sum of Gibbs free energy for the overall mechanism is 4.92 eV, which is the Gibbs free energy for water redox reaction

pH	ΔG_1 (eV) [R1]	ΔG_2(eV) [R2]	ΔG_3 (eV) [R3]	ΔG_4 (eV) [R4]	η (V)
pH=0	1.25	-3.54	1.36	-1.56	0.13
pH=7	0.50	-4.29	0.61	-2.31	-

Charge Carrier Mobility

For calculation of charge carrier mobility, we have used the Lang et al.[5] robust formalism:

$$\mu_x = \frac{e\hbar^3 \left(\frac{5C_x + 3C_y}{8}\right)}{k_B T (m_x)^{\frac{3}{2}} (m_y)^{\frac{1}{2}} \left(\frac{9E_{1x}^2 + 7E_{1x}E_{1y} + 4E_{1y}^2}{20}\right)} \times 10^4 \, cm^2 V^{-1} s^{-1}$$

Here, $\hbar$ is the reduced Planck constant, e is the charge of electron, k_B is the Boltzmann's Constant, m_x and m_y are the effective masses of electron/hole, C_x and C_y are the elastic modulus along x & y directions, respectively and $E_x = E_y = E_{DP}$ is the deformation potential and T is the absolute temperature in Kelvin (Here T = 298 K). Both the charge carriers have sufficiently

high mobility to support the photocatalytic activity of the blue-AsP monolayer. Anisotropic carrier mobilities favor charge separation and reduce their recombination.

Table S2. The elastic constant (C_x and C_y), deformation potential (E_x and E_y), electron and hole effective masses (m_x and m_y) in terms of m_0 (rest mass of an electron), and carrier mobilities (μ_x and μ_y) in x and y directions

Charge Carrier	C_x	C_y	E_x	E_y	m_x	m_y	μ_x	μ_y
e	67.741	67.741	-6.39	4.65	0.612	0.63	309.99	494.04
h	67.741	67.741	-3.7	-3.73	0.161	0.499	2305.14	740.75

References:

1 X. Cai, Y. Chen, B. Sun, J. Chen, H. Wang, Y. Ni, L. Tao, H. Wang, S. Zhu, X. Li and et al., Two-dimensional Blue-AsP monolayers with tunable direct band gap and ultrahigh carrier mobility show promising high-performance photovoltaic properties, *Nanoscale*, 2019, **11**, 8260–8269.

2 H. Y. Chen, M. Palummo, D. Sangalli and M. Bernardi, Theory and Ab Initio Computation of the Anisotropic Light Emission in Monolayer Transition Metal Dichalcogenides, *Nano Lett.*, 2018, **18**, 3839–3843.

3 C. He, J. H. Zhang, W. X. Zhang and T. T. Li, Type-II InSe/ g-C3N4 Heterostructure as a High-Efficiency Oxygen Evolution Reaction Catalyst for Photoelectrochemical Water Splitting, *J. Phys. Chem. Lett.*, 2019, **10**, 3122–3128.

4 J. K. Nørskov, J. Rossmeisl, A. Logadottir, L. Lindqvist, J. R. Kitchin, T. Bligaard and H. Jónsson, Origin of the overpotential for oxygen reduction at a fuel-cell cathode, *J. Phys. Chem. B*, 2004, **108**, 17886–17892.

5 H. Lang, S. Zhang and Z. Liu, Mobility anisotropy of two-dimensional semiconductors, *Phys. Rev. B*, 2016, **94**, 235306.